Science of the Total Environment 967 (2025) 178814

Contents lists available at ScienceDirect

Science of the Total Environment

journal homepage: www.elsevier.com/locate/scitotenv

Quantification of turbid wakes in offshore wind farms using satellite remote sensing

Enora M. Lecordier [a,*], Pierre Gernez [b], Krysia Mazik [c], Katharine York [d], Rodney M. Forster [e]

[a] Energy and Environment Institute, University of Hull, Hull, UK
[b] Nantes Université, Institut des Substances et Organismes de la Mer, ISOMER, UR 2160, F-44000 Nantes, France
[c] School of Environmental Sciences, University of Hull, UK
[d] Offshore Renewable Energy Catapult, Grimsby, UK
[e] Hull Marine Laboratory, School of Environmental Sciences, University of Hull, UK

HIGHLIGHTS

- Satellite images quantified the presence of turbid wakes in offshore wind farms.
- Sediment increased downstream of wind turbine foundations.
- A clear seasonal pattern in wake formation was observed.
- Wake strength was explained by foundation type, bathymetry, hydrodynamics, and wind.

GRAPHICAL ABSTRACT

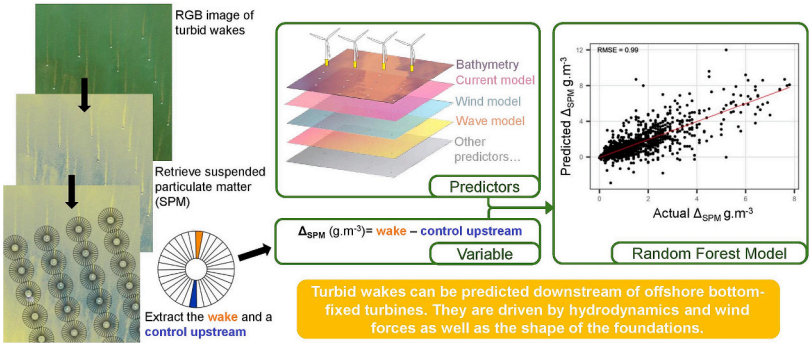

ARTICLE INFO

Editor: Meng GAO

Keywords:
Turbid wakes
Hydrodynamics
Suspended particulate matter
Offshore wind
Geospatial analysis
Satellite remote sensing

ABSTRACT

The offshore wind (OSW) industry is expanding globally, particularly in areas of shallow water such as the North Sea. The environmental impacts of large-scale offshore development are not yet well understood. Satellite remote sensing has shown an increase in suspended particulate matter (SPM) concentration in the wake of wind turbines' foundations due to turbulence in the current flow when encountering the structures. High-resolution Sentinel-2 and Landsat-8/9 satellite observations were used to quantify sediment concentration in the wakes at a range of sites across the southern North Sea. The sites studied had different water depths as well as different types of foundations, and different hydrodynamic conditions, allowing a variety of forcing factors to be related to observed sediment wake intensity. A Random Forest model was built to predict the increase in the amount of suspended sediment observed in wakes downstream of a foundation. Foundation types of large diameter such as gravity-based and monopile produced more intense wakes than jacket foundations. Also, sediment wake intensity followed a seasonal pattern, where the highest SPM concentration was observed during spring. The main factors driving sediment wake intensity are the synergy of wind and hydrodynamic forces alongside the concentration of suspended sediment already present in the area. When turbid wakes are present, increased surface sediment concentration inside and downstream of OSW farms is likely to reduce underwater light availability. This study

* Corresponding author.
E-mail address: e.m.lecordier-2021@hull.ac.uk (E.M. Lecordier).

https://doi.org/10.1016/j.scitotenv.2025.178814
Received 13 September 2024; Received in revised form 22 December 2024; Accepted 8 February 2025
Available online 12 February 2025

showed that sediment concentration within turbid wakes can be quantified and predicted by employing the knowledge of the structure's construction type and environmental conditions.

1. Introduction

Offshore wind (OSW) energy has been widely accepted as a major part of the change to renewable energy required to support Net Zero objectives and tackle climate change (Fitch-Roy, 2015; IPCC, 2011). This acceptance is leading to an explosive development of the OSW industry in areas of shallow depth and suitably reliable wind conditions, such as the North Sea, Yellow Sea, and South China Sea. In the North Sea, >2600 turbines were installed and producing power by late 2022 (Chirosca et al., 2022; Zhang et al., 2021). Due to its wind resource and shallow waters, the North Sea is by far the most active part of the world in this field with European leaders such as the UK, Germany, The Netherlands, Denmark and Belgium (Fitch-Roy, 2015). The wind industry expansion has been accompanied by large increases in engineering research and development to optimise wind harvesting and electrical energy distribution and storage (Chen and Kim, 2021). However, the current understanding of the environmental impacts of OSW lags somewhat behind the advances in design and operations. One important aspect of OSW-environment interaction is an alteration in hydrodynamic conditions as tidal flow moves water through a wind farm (Rogan et al., 2016). The largest sites may consist of several hundred turbines and their foundations, with each structure interacting with the water flow. The type of structure used to support wind turbines and their blades varies across sites. In 2019, monopiles represented a majority of the bottom-fixed foundation type in Europe with 81 % followed by jackets (9 %), gravity-based (6 %), tripods and tripiles together (4 %) (Negro et al., 2017; WindEurope, 2020). This trend has continued as monopiles are the easiest foundation to manufacture and install in shallow waters of <50 m depth.

As underwater structures of several meters in diameter, OSW foundations are known to disturb the water flow: erosion of sediment at the base, reduced current velocities and increased turbulence were recorded downstream of model turbines (Miles et al., 2017; Schendel et al., 2018; Welzel et al., 2019). Changes in water flow around the structure can be visualised in the form of linear turbid wakes downstream of the foundations and aligned with the current direction (Baeye and Fettweis, 2015). Turbid wakes can be 30–150 m wide and several kilometres long (Vanhellemont and Ruddick, 2014) and are characterised by an increase in suspended particulate matter (SPM) concentration at the surface (Forster, 2018; Reichart et al., 2017). Wake appearances are proof of a disturbed environment with an increased mixing of water layers, known to cause an upward movement of suspended sediment throughout the water column, especially in the upper half (Austin et al., in-press; Bailey et al., 2024). Floeter et al. (2017) showed that in stratified waters, the underwater structures increased the vertical mixing, disturbing the thermocline and leading to a lower sea surface temperature (by 1 to 2 °C) inside and for a few kilometres downstream of a wind farm. Also, the current velocity within the wind farm can be reduced (Cazenave et al., 2016). As the water flow encounters the foundation structure, a scour hole can appear at the base of the foundation (Matutano et al., 2013; Sumer et al., 2001). To mitigate this effect, scour protections can be placed at the bottom of the supporting structures such as concrete mattresses (between 0.15 m to 0.45 m thickness) or rock armouring (EGS International Ltd, 2016; Pipeshield, 2024). At the scale of a whole wind farm and its surroundings, the increase in SPM concentration due to wake effects, may or may not be significant, as described by Brandao et al. (2023) using a Before-After Control-Impact approach allowing the analysis of a potential impact by observing changes in time (Before-After) and space (Control-Impact). There are pronounced seasonal and spatial variations in SPM concentration in coastal seas (Eleveld et al., 2008). However, as established previously, turbid wakes do change the local water quality at the scale of a single turbine and for some distance downstream with a potential cumulative effect between turbines. This increase in SPM concentration could potentially affect light-dependent ecological processes (primary productivity, sight-based feeding), especially in the context of biodiversity hot spots due to the reef effect, yet the factors controlling the intensity of these wakes have not been quantified. Changes in primary production would disrupt the structure of the food chain and reduce carbon sequestration. To study this local effect, SPM observation at a high spatial resolution (i.e. < 100 m) is required (Vanhellemont and Ruddick, 2014). Most of the existing OSW farms are built in regions under semi-diurnal tidal current conditions meaning that a turbid wake can be generated in one direction for a maximum of 6 h, after which the tidal flow reverses and a new wake may be visible in the opposite direction.

Accordingly, turbid wakes present short-term temporal and spatial characteristics. The use of Sentinel-2 and Landsat-8/9 satellites, as a virtual constellation, has allowed sufficient temporal and spatial resolution to study turbidity in aquatic environments in several studies (Kuhn et al., 2019; Maciel and Pedocchi, 2021; Wang et al., 2021). While those studies have documented SPM concentration in inland or coastal waters, using this virtual constellation for discontinuous sediment load can be challenging as the wake direction differs from one image to another depending on the current direction, making it difficult to observe. The present study aims to quantify the SPM concentration of turbid wakes and determine the physical and environmental forces under which they occur, associated with typical OSW structures. This will be done by comparing contrasting sites, differing in their range of bathymetry and type of foundation, with a variable tidal regime. This quantification of OSW on sediment concentration in the water column could help support environmental impact assessment for future wind farms, and add to the knowledge pool for the addition of other marine activities in the area, which can be impacted by SPM concentration variability.

2. Material and methods

2.1. Study areas

As a preliminary screening study and to select sites of interest, 33 North Sea wind farms in Belgian and British waters were considered. For each one of them, 30 high-resolution Sentinel-2 cloud-free satellite ocean colour scenes between 1st September 2019 and 1st March 2024 were inspected visually using the Sentinel Hub EO Browser (https://apps.sentinel-hub.com/eo-browser/). The number of scenes where at least one sediment wake was visible within the wind farm was reported as the relative occurrence (percentage of satellite scenes with wakes out of 30 images, Fig. 1). Turbid wakes were regularly observed in the Humber and Thames areas, but less so in the Tyne area (Fig. 1a and b). Within the Humber area, Lincs, Lynn, and Inner Dowsing wind farms were selected for their similar location but different numbers of wakes (respectively 90 %, 70 %, and 50 %). In Belgium, turbid wakes were also regularly observed. The selected wind farms were Norther, Rentel, Thornton Bank Phase I, II, and III, located next to each other, with respectively 77 %, 73 %, 67 %, 60 %, and 50 % wakes recorded (Fig. 2). The selected sites contain a variety of foundation types, and also have regular cloud-free images and are located on complete satellite tiles, facilitating their study. Also, the selected OSW farms had easily accessible environmental impact assessments and post-construction surveys providing details on the type of foundation and diameter. Details on regional environmental conditions where the studied wind farms are located are given in Supplementary Table S.1.

2.1.1. OSW in the Belgian Part of the North Sea

The Belgian Part of the North Sea (Figs. 1b and 2a) contains OSW farms over a great range of water depths with different types of foundations only a few kilometres from each other (Table 1). The study site comprises five wind farms at a distance between 24 and 38 km from shore. The area is characterised by low turbidity with an average surface SPM concentration of 4.6 g m^{-3} with values ranging from 2.8 to 7.1 g m^{-3} (Fig. 2a). The principal wind direction is from the south-west with a mean wind speed of 7 m · s^{-1} at 10 m height (Baeye et al., 2011; Global Wind Atlas 3.0, 2023). Van den Eynde et al. (2010) recorded the tidal current running from north-east to south-west and vice-versa, parallel to the coastline with a range of 0.3 to 0.9 m.s^{-1} during the summer. The sea floor is mostly composed of medium sand with a particle size of 250–500 μm (Hademenos et al., 2019; Kint et al., 2020). The wind farms are installed across a wide range of bathymetry from 9 to 36 m (Fig. 2c).

2.1.2. OSW sites off Lincolnshire, UK

The second study site, off Lincolnshire (UK, Fig. 1b and 2a), is composed of three wind farms located between 5 and 11 km offshore (Table 1). Unlike the Belgian site, the average surface SPM concentration in the Lincolnshire site is high: about 27.4 g m^{-3} on average with values ranging from 16.7 to 36.3 g m^{-3} (Fig. 2a). The wind farms are constructed over sand to sandy-gravel seabed (EGS International Ltd, 2017b; RPS, 2014), in shallow waters (depth from 7 to 26 m, Fig. 2.b). The tidal current runs along the coastline (north-south orientation) and the peak tidal current varies from 1 to 1.3 m · s^{-1} (RPS, 2014). The main wind direction is south-west with 7.6 m · s^{-1} on average at 10 m height (Global Wind Atlas 3.0, 2023).

2.2. Data acquisition and processing

2.2.1. Satellite images

The European Space Agency (ESA) launched the Sentinel-2 twin satellites in 2015 and 2017 (respectively, Sentinel-2A and Sentinel-2B). The optical Multi-Spectral Instrument (MSI) image data was accessed using the "SEN2R" library in R (Ranghetti et al., 2020). NASA launched Landsat-8 in 2013 and Landsat-9 in 2021. The Operational Land Imagers (OLI) Collection 2 data, with 30 × 30 m resolution, were acquired from the United States Geological Survey (https://earthexplorer.usgs.gov/). For both Sentinel and Landsat, orthorectified and terrain-corrected Level-1 data were downloaded from 1st January 2019 to 30th June 2023 for scenes with <10 % cloud cover. Satellite images were recorded between 10:55 and 11:15 for Sentinel-2 and 10:40 and 10:40 for Landsat. Atmospheric correction (AC) was done with ACOLITE, developed by the Royal Belgium Institute of Natural Sciences (RBINS) and freely available from https://github.com/acolite/acolite. A "dark spectrum fitting" (DSF) atmospheric correction method was chosen and applied to the whole area followed by a sun glint correction (Vanhellemont, 2019). Non-water pixels were masked when top of atmosphere (TOA) reflectance, ρt, exceeded 0.0215 in the short-wave infrared (SWIR) band centred at 1600 nm. Once AC was applied, SPM concentration was retrieved using Nechad's algorithm (Eq. (1)) as it was shown to perform satisfactorily in both offshore and near-shore waters (Luo et al., 2018; Nechad et al., 2010):

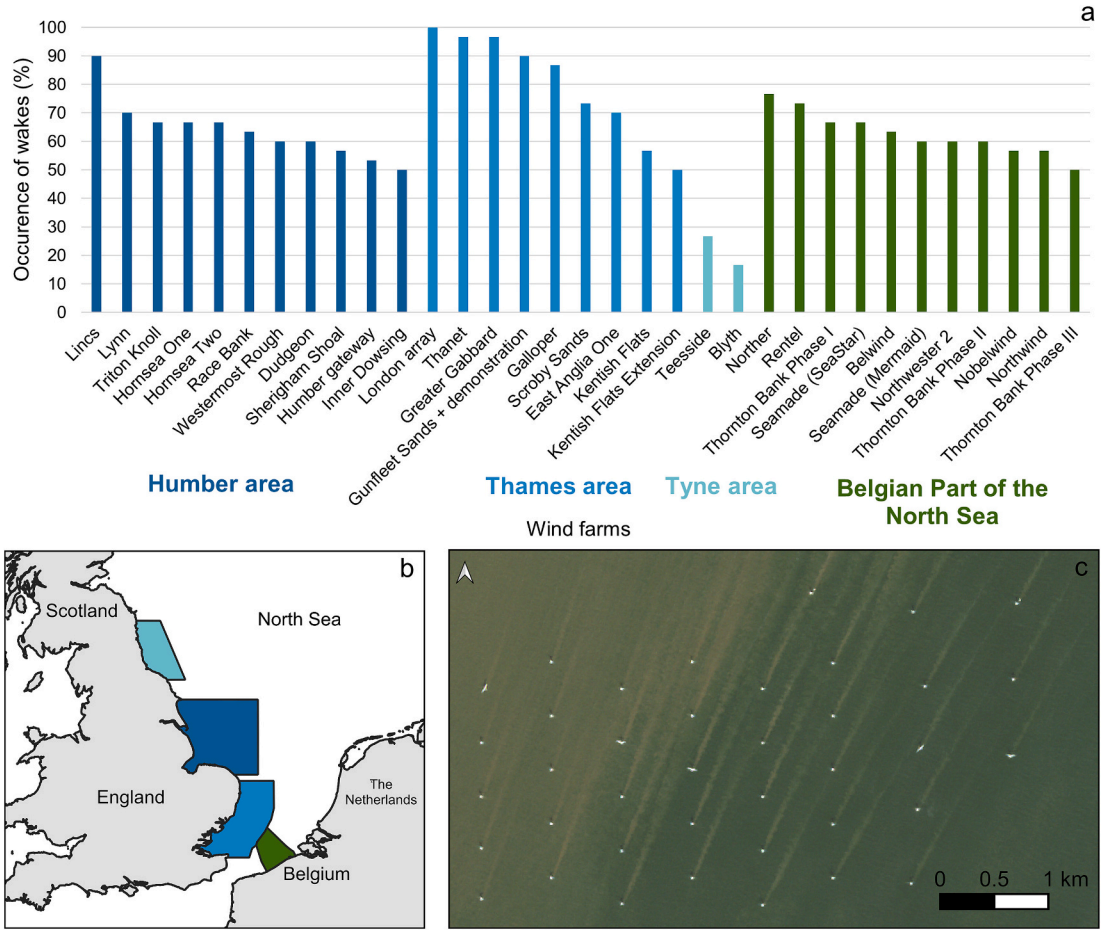

Fig. 1. (a) Occurrence of sediment wakes out of 30 cloud-free Sentinel-2 scenes for eastern England and Belgian wind farms. (b) Location of the wind farms studied: three British areas (blue shades) and the Belgian part of the North Sea (green). (c) An example of sediment wakes within Lynn and Lincs wind farms (Humber area, UK) visible on a Sentinel-2B scene (date of acquisition 23/05/2023).

$$SPM\ (g.m^{-3}) = \frac{A^{\rho} * \rho_w}{1 - \left(\frac{\rho_w}{C^{\rho}}\right)} \quad (1)$$

where ρ_w represents the water-leaving radiance in the red part of the visible spectrum (i.e. corresponding to spectral bands at 655 and 665 nm for Landsat-8/9 and Sentinel-2, respectively), and A^{ρ} and C^{ρ} are band-specific and sensor-specific calibration coefficients (Nechad et al., 2010; Vanhellemont, 2019). To use the two satellites in synergy, Sentinel-2 scenes have been rescaled at 30 × 30 m resolution to match that of Landsat, instead of its 10 × 10 m native resolution. A post-processing quality control was carried out to keep only cloud-free and storm-free images (showing areas of white-capped waves), yielding a total of 19 Sentinel-2 and 9 Landsat-8/9 images for the British site, and 24 Sentinel-2 and 10 Landsat-8/9 images for the Belgian site (Table 2). Suitable images were more frequent in spring and summer (38 scenes) than in autumn and winter (22 scenes).

To complement the analysis, the downwelling diffuse attenuation coefficient spectrally integrated over the visible range (K_dPAR) was also retrieved using ACOLITE for each satellite image using the updated version of Lee et al. (2002).

2.2.2. Bathymetry

European Marine Observation and Data Network (EMODnet) provides standardised and quality-controlled marine data across Europe and allows the downloading of comparable bathymetric data for both the UK and Belgium sites. The EMODnet DTM 2022, complemented by the general bathymetric chart of the oceans (GEBCO), provides bathymetry data at a 115 m grid resolution. This data allowed the acquisition of water depth information, Z, for each turbine location. The bathymetry was also converted into a slope value in % over the area. The

Table 1
Selected wind farms in Belgium (BE) and the United Kingdom (UK), listed in chronological order of construction, and type of structure supporting these turbines.

Name (country)	Turbines	Area (km^2)	Distance to shore (km)	Fully commissioned
Lynn (UK)	27 monopiles	8	6.2	01/03/2009
Inner Dowsing (UK)	27 monopiles	9	6.9	01/03/2009
Thornton Bank Phase I (BE)	6 gravity-based	0.4	26.6	10/05/2009
Thornton Bank Phase II (BE)	30 jackets (4 pin piles)	12	26.2	31/01/2013
Thornton Bank Phase III (BE)	18 jackets (4 pin piles)	7	26.7	18/09/2013
Lincs (UK)	75 monopiles	38	9.5	27/09/2013
Rentel (BE)	42 monopiles	23	30.5	31/12/2018
Norther (BE)	44 monopiles	38	22.0	01/06/2019

Table 2
Number of cloud-free satellite scenes available for each site, listed per season: winter (December–February), spring (March–May), summer (June–August), and autumn (September–November).

	Winter	Spring	Summer	Autumn
United-Kingdom	5	10	7	6
Belgium	7	12	11	4

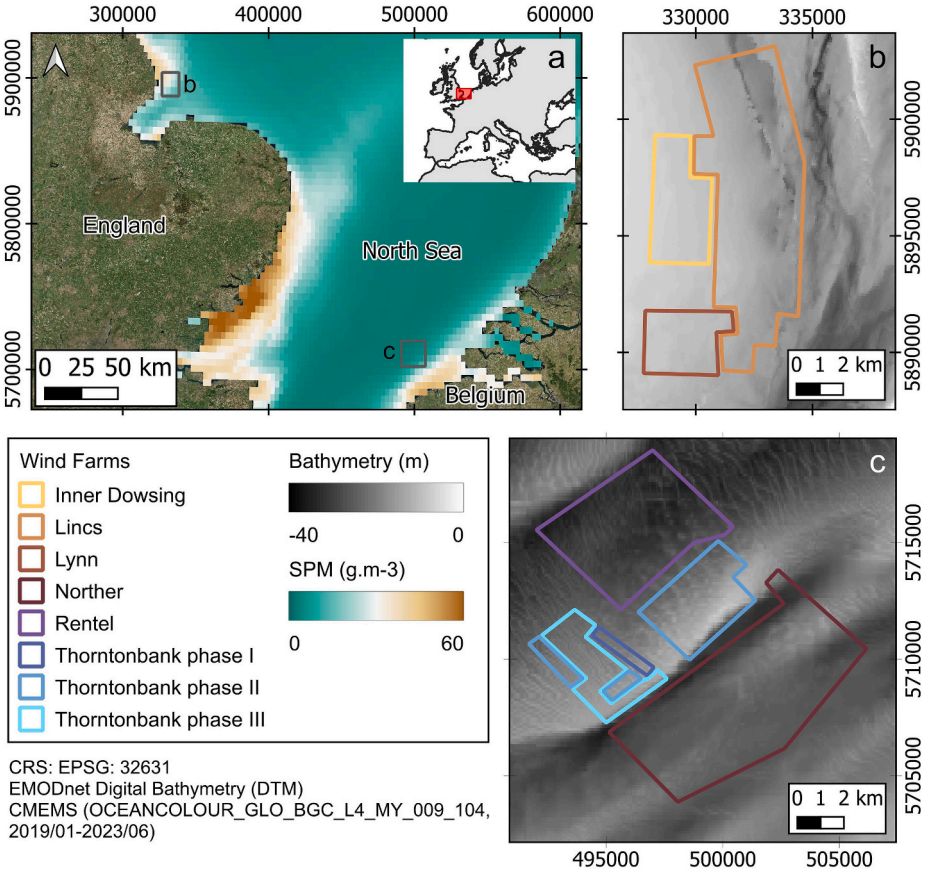

Fig. 2. (a) Monthly averaged suspended particulate matter (g.m^{-3}) from January 2019 to June 2023 in the North Sea. Studied wind farm layouts in (b) the UK and (c) Belgium are displayed on top of bathymetry.

mean slope (%), μ_{slope}, was obtained by averaging the slope in a 1 km radius around the structure, to give insight into the seabed morphology.

2.2.3. Environmental variables from Copernicus

This study has been conducted using E.U. Copernicus Marine Service (CMEMS) spatial information. CMEMS provides a wide range of worldwide environmental data from modelling, in-situ data and satellite observations.

The Atlantic - European North West Shelf - Ocean Physics Analysis and Forecast model (product: NORTHWESTSHELF_ANALYSIS_FORECAST_PHY_004_013, dataset: MetO-NWS-PHY-hiCUR) contained hourly products for current speed and direction over a 1/36° grid resolution (approximately 2–3 km per cell). The closest current velocity and direction in time from each scene were acquired from surface to bottom (0 m, 3 m, 5 m, 10 m, 15 m, 20 m, 25 m, 30 m, and 40 m depth). The current direction was later used to narrow down the wakes' location.

The Atlantic - European North West Shelf - Ocean Wave Analysis and Forecast (product: NORTHWESTSHELF_ANALYSIS_FORECAST_WAV_004_014, dataset: MetO-NWS-WAV-hi) contained hourly products for wind wave and swell data on a 1/36° grid resolution (approximately 2–3 km per cell). The closest wind wave and swell heights (m) and directions (°) in time from each scene were downloaded.

The Global Ocean Daily Gridded Sea Surface Winds from Scatterometer (product: WIND_GLO_ PHY_L4_NRT_012_004, dataset: cmems_obs-wind_glo_phy_nrt_l4_0.125deg_PT1H) contained hourly wind conditions Level-4 data at 10 m height from 1st July 2020 at 0.125° × 0.125°. This data corresponds to the Advanced Scatterometer (ASCAT) aperture radar satellite, Metop-B and Metop-C constellation launched in 2012 by the European Organisation for the Exploitation of Meteorological Satellites (EUMETSAT). For each satellite scene, the corresponding wind conditions, such as velocity (v_{wind}), and direction, on that date and time were acquired.

The Global Ocean Colour (Copernicus-GlobColour), Bio-Geo-Chemical, L4 (monthly and interpolated) from Satellite Observations (1997-ongoing) (product: OCEANCOLOUR_GLO_BGC_ L4_MY_009_104, dataset: cmems_obs-oc_glo_bgc-transp_my_l4-multi-4km_P1M) contained monthly satellite ocean-colour derived SPM concentration data on 4 km × 4 km resolution. Monthly data from January 2019 to June 2023 have been downloaded and averaged for producing a map of the background SPM concentration in the North Sea (Fig. 2a).

The "CopernicusMarine" R library allowed the automatic download of data from the CMEMS website (https://data.marine.copernicus.eu/products). From the Copernicus dataset, several parameters were used. First, the significant wind wave height H_{ww} and swell height H_{swell} were directly extracted. To understand the effect of the interaction between swell and wind waves, an angle α_{sww} was computed as the difference between swell and wind wave direction, where 0° means that both are going in the same direction and 180° means that both are going in the opposite direction). Then, to understand the interaction between the wind and current direction, an angle α_{cw} was computed in the same way as α_{sww}.

2.2.4. Supporting structure specifications

The type of foundations and the diameter of each structure were found in the literature (Table 3). In the case where information was missing on turbine diameter, assumptions had to be made according to the known foundation of each farm (Norro, 2018). Knowing the diameter of each foundation and the current speed condition at the bottom, the Reynolds number (*Re*) has been computed, for each turbine on each satellite scene using Eq. (2).

$$Re = \frac{\rho^* u^* L}{\mu} \tag{2}$$

where ρ is the density of the fluid (kg · m^{-3}) which is commonly 1.025 for seawater, u is the current velocity (m · s^{-1}), L is the diameter of the base of the foundation (m), and μ is the dynamic viscosity of the fluid (N · s m^{-2}). μ was 0.0013076, computed for seawater at 10 °C and remained constant (The Engineering ToolBox, 2004). For the jacket foundation, the structure presented a high pile-diameter-to-gap ratio (G/D) of 9 (2 m pile legs spaced 18 m apart, Bolle et al., 2012). When G/D > 5, the piles can be considered free of flow interaction with each other (Amini et al., 2012; Welzel et al., 2024). Still, the cumulative impact on sediment resuspension of the 4 pile legs is unknown if the flow becomes turbulent. Therefore, only one pin leg was considered for computing the *Re* number in this study.

Table 3
Turbine specifications per wind farms.

Wind farm	Type of foundation (4C Offshore, 2022)	Foundation diameter (m) at the base	References
Lynn	Monopile	4.74	(RPS, 2014; Sif, 2024)
Inner Dowsing	Monopile	4.74	(RPS, 2014; Sif, 2024)
Thornton Bank Phase I	Gravity based	23.5	(C-Power, 2024; Peire et al., 2009)
Thornton Bank Phase II	Jacket	2 (for each pin pile)	(Bolle et al., 2012, 2013; C-Power, 2024)
Thornton Bank Phase III	Jacket	2 (for each pin pile)	(Bolle et al., 2012, 2013; C-Power, 2024)
Lincs	Monopile	4.7	(EGS International Ltd., 2016, 2017a; RPS, 2014; Sif, 2024)
Rentel	Monopile	7.5 (10 piles), 7.8 (26), 8 (6)	(Norro, 2018; Sif, 2024)
Norther	Monopile	7.2–7.8 averaged to 7.5	(Norro, 2018)

2.2.5. Turbid wake extraction

The location of each structure was found using data from Hoeser et al. (2022) who identified wind turbine locations using Sentinel-1 SAR satellite images. To isolate the effect of environmental parameters on turbid wake intensity, the selected structures were chosen to not be located in the wake of a neighbouring one, for any current direction. To do so, turbines were sampled only if they were not sheltered by another one, according to where the current was coming from: north-east (0–90°), south-east (90–180°), south-west (180–270°), or north-west (270–360°) (Fig. 3). This sheltering phenomenon was more problematic for the Belgian wind farms where sampling needed a cautious study of satellite scenes, and 26 turbines could not be used in any current conditions. Also, gravity-based foundations could only be sampled when the current was coming from the north-east. The problem was less impactful in the UK where turbines were rarely in the wake of another one for most current conditions. However, when the current came from the north-west, only 11 turbines were suitable (Fig. 3a). The total of turbines sampled for each current direction is presented in Supplementary Table S2.

To avoid the structure's own shadow altering the water-leaving radiance, a mask was built on a winter Sentinel-2 scene in the Lincolnshire site as the shadow would be the longest due to the site being north and the sun being low. The best mask fit was found to be a rectangle of 75 × 250 m north-north-west of the turbines. As Sentinel-2 and Landsat-8/9 pass around the same time of the day (approximately 10:50 UTM), the same mask was used for both sites and satellite missions.

Finally, around every turbine, a circular buffer of 100 m inner diameter and 350 m outer diameter was generated. This buffer was far enough away to avoid the potential shadow of the turbines but could not be longer without overlapping with the wake of a neighbouring turbine. This buffer was divided into 32 equal "wedges" fitting the wake's

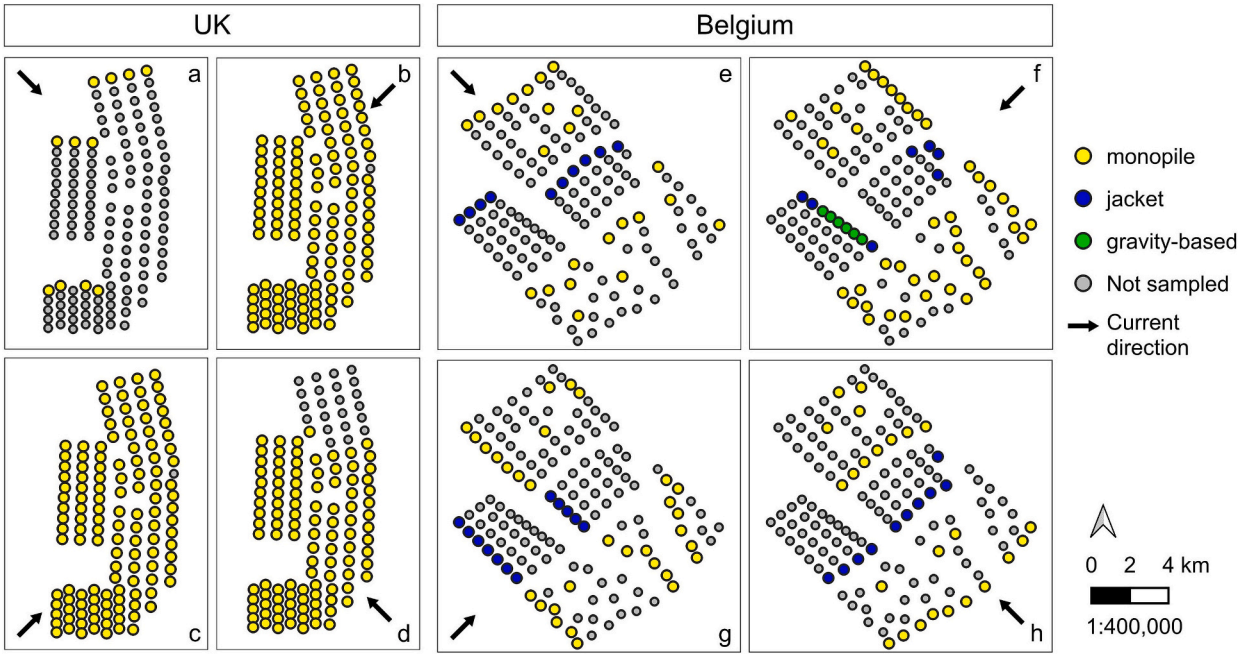

Fig. 3. Sampled turbines for each current direction case: north-west (a, e), north-east (b, f), south-west (c, g), and, south-east (d, h), and north-east, for the British (left) and the Belgian (right) sites.

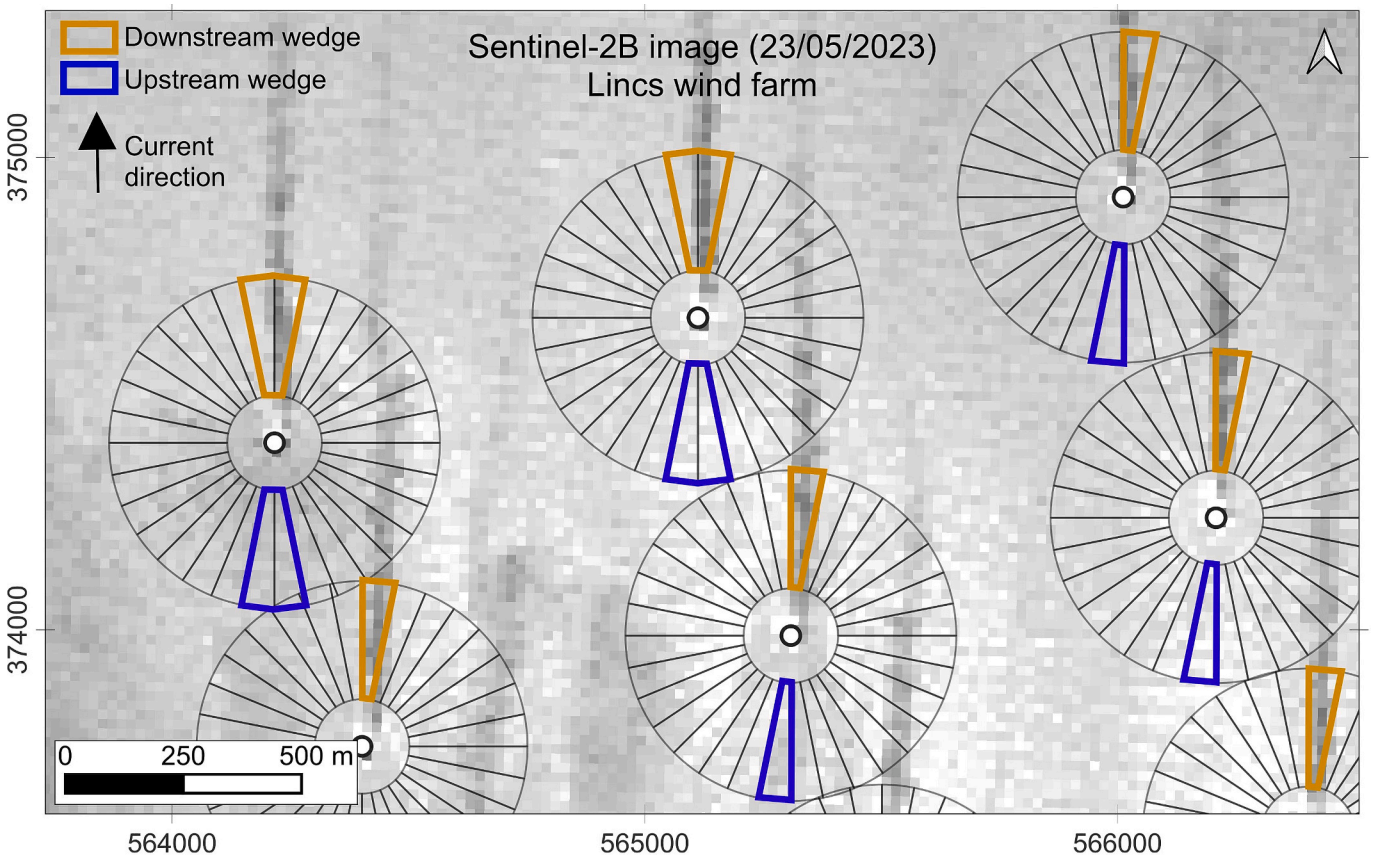

Fig. 4. Sentinel-2B SPM concentration scene (acquisition date: 23/05/2023) illustrating the wedges methodology to sample turbid wakes. In this case of northward current, the orange wedges correspond to the wedges sampled downstream containing the wake. The blue wedges are on the upstream side of the turbine and correspond to the background SPM concentration. In the case of wake overlapping wedges, two wedges were sampled on each side.

general width (Fig. 4). With an image resolution of 30 m × 30 m, each wedge contained about 16 pixels. The turbine location identifications, turbine samplings regarding current direction, shadow mask and wedges creation were conducted using QGIS (Buenos Aires 3.26, QGIS.org, 2024). For each turbine, the current direction indicated the wedge where a turbid wake was more likely to occur. Because the wedges were quite thin (11.25°), 5 other wedges on each side were also sampled in case of mismatch with the current model. Only the wedge containing the highest averaged SPM concentration was retained and deemed to be the one containing the turbid wake. However, if the averaged SPM concentration value within one of the two wedges on each side was >99 % of the one retained initially, the wake was considered to be straddling two wedges. In that case, both wedges were sampled (Fig. 4). Then, the corresponding upstream wedge (or wedges in the case of overlapping wake) on the opposite side of the structure were sampled as the background SPM concentration. The averaged background SPM concentration (SPM_b) was subtracted from the downstream SPM concentration (SPM_d), corresponding to the wake, to obtain the absolute difference, Δ_{SPM}, characterising the wake intensity (Eq. (3)). Finally, the relative SPM difference ($\%_{SPM}$) corresponding to the percentage increase in SPM concentration produced by each turbine was calculated (Eq. (4)). The same process was followed to extract K_{dPAR} from the wake. K_{dPAR} was used to retrieve the depth of the euphotic zone (Z_{eu}) defined as the depth where the underwater PAR equals 1 % of the incident reaching the water surface. The potential decrease in Z_{eu} was then computed following the same calculation as $\%_{SPM}$.

$$\Delta_{SPM} = SPM_d – SPM_b \tag{3}$$

$$\%_{SPM} = \frac{SPM_d - SPM_b}{SPM_b} * 100 \tag{4}$$

The wedge selection and pixel extraction were performed using R (version 4.2.1, R Core Team, 2024).

2.2.6. Statistics

Seven outliers were removed from the dataset. These extreme values were due to the engine wake of maintenance vessels operating on the turbines either upstream or downstream leading to abnormally high reflectance, and hence higher SPM concentration values. Two aspects of the wakes were studied with statistics. First, the significant difference between SPM_b and SPM_d for each turbine was investigated, within each wind farm, for every type of foundation and during each season separately to know if sediment wakes were present in each case. The data were paired (due to measurement of SPM concentration upstream and downstream of a structure in the water column) but were not normally distributed. Therefore, the Wilcoxon signed-rank test was used. Then, the second metric studied was the relative increase in SPM concentration ($\%_{SPM}$) produced by the turbines to know if some wind farms, types of foundations or seasons favoured a higher sediment wake intensity. The Kruskal-Wallis test was used to identify a potential dominance between the variables followed by the Dunn's Test (using the Bonferroni method) to identify which variables were most important (Dinno, 2015; Dunn, 1961). Again, wind farms, types of foundations and seasons were studied separately.

Then, a random forest (RF) model was computed to predict the Δ_{SPM} of a turbine. An RF model is a supervised classifier based on decision trees that can handle non-linear data, and unbalanced and noisy training samples (Belgiu and Drăguţ, 2016; Gislason et al., 2006). The model was built and trained with the following parameters: SPM_b ($g \cdot m^{-3}$), α_{sww} (°), α_{cw} (°), Re, H_{swell} (m), H_{ww} (m), μ_{slope} (%), Z (m), and v_{wind} ($m \cdot s^{-1}$). The processing and statistics were done using R (version 4.2.1, R Core Team, 2024). The RF model was developed with ntree = 500 (Lawrence et al., 2006) and mtry = 3 on two-third of the dataset (2971 turbines) and tested on the last third (1485 turbines) using the 'randomForest' package developed by Breiman (2001). The importance of each variable was assessed using the percentage increase mean squared error (MSE), and the total increase in node purities calculated from the Gini impurity index commonly used for computing the splits in trees.

3. Results

3.1. Variability between wind farms

SPM concentration was significantly higher downstream than upstream of the turbine, regardless of the wind farm (Wilcoxon Test p-values <0.0001, Fig. 5a). On average, the relative SPM concentration increase in Belgian waters (values ranging from 5 % to 9.6 %) was lower than in the UK wind farms (values ranging from 7.9 % to 10.9 %, Fig. 5b). In Belgium, the relative SPM concentration increase in Thorntonbank Phase I (9.6 %) was higher than Rentel (7.1 %), Thornton Bank Phase II (5 %) and Thornton Bank Phase III (6 %, Dunn's Test p-value <0.05). In the UK, the relative SPM concentration increase in Inner Dowsing (7.9 %) was lower than Lincs (10.9 %) and Lynn (10.9 %, Dunn's Test p-value <0.001).

3.2. Effect of the type of foundation

The influence of foundation type was assessed for the Belgian site, as it contains three different types of foundation (Table 3). SPM concentration was significantly higher downstream than upstream of the wind farm, whatever the foundation type (Wilcoxon p-values <0.0001, Fig. 6.a). Overall, the relative SPM concentration difference was higher downstream of gravity-based and monopile foundations (respectively, 9.3 % and 7.9 %, Fig. 6.b) than of jacket foundations (5.4 %, Dunn's Test p-values <0.001).

3.3. Effect of seasonality

Background SPM concentration varied seasonally at both sites, with a winter maximum and a summer minimum (Fig. 7a). SPM concentration was significantly higher downstream than upstream of the wind farm, whatever the season (Wilcoxon p-values <0.0001). In Belgium, during autumn, the relative SPM concentration increase (4.3 %) was lower than during the rest of the year (8.4 % during winter, 9.2 % during spring, and 6.6 % during summer, Dunn's Test p-value <0.001, Fig. 7.b). In the UK, the SPM concentration increase was higher during spring than during summer (9.1 %) and autumn (9.4 %, Dunn's Test p-value <0.05).

3.4. Random forest model

The RF model was developed to identify which physical and environmental parameters best explain the intensity of sediment wakes and predict their intensity. From a practical point of view, the model could be used by developers or regulatory agencies to predict the quantity of SPM concentration resuspended by a wind turbine foundation. The RF model explained 63.12 % of the SPM concentration variability, with an RMSE of 0.99 between the predicted and actual Δ_{SPM} values (Fig. 8). The most important variables driving the intensity of the wake are the background SPM concentration (SPM_b), and the difference between the swell and wind wave direction (α_{sww}, Fig. 9). Those variables showed the highest percentage of increase in MSE (%IncMSE), corresponding to the relative increase of the MSE if the variable was removed from the model. These variables also show the highest increase in node purity (IncNodePurity), making them very good discriminants in the decision tree.

3.5. Presence and absence of wakes

In some cases, a significant difference in wake intensity was observed between turbines close to each other. For example, Fig. 10 showed a sequential increase in sediment wake intensity from turbines D8 to D2. However, turbines D1 and D0 showed very reduced or absence of wake

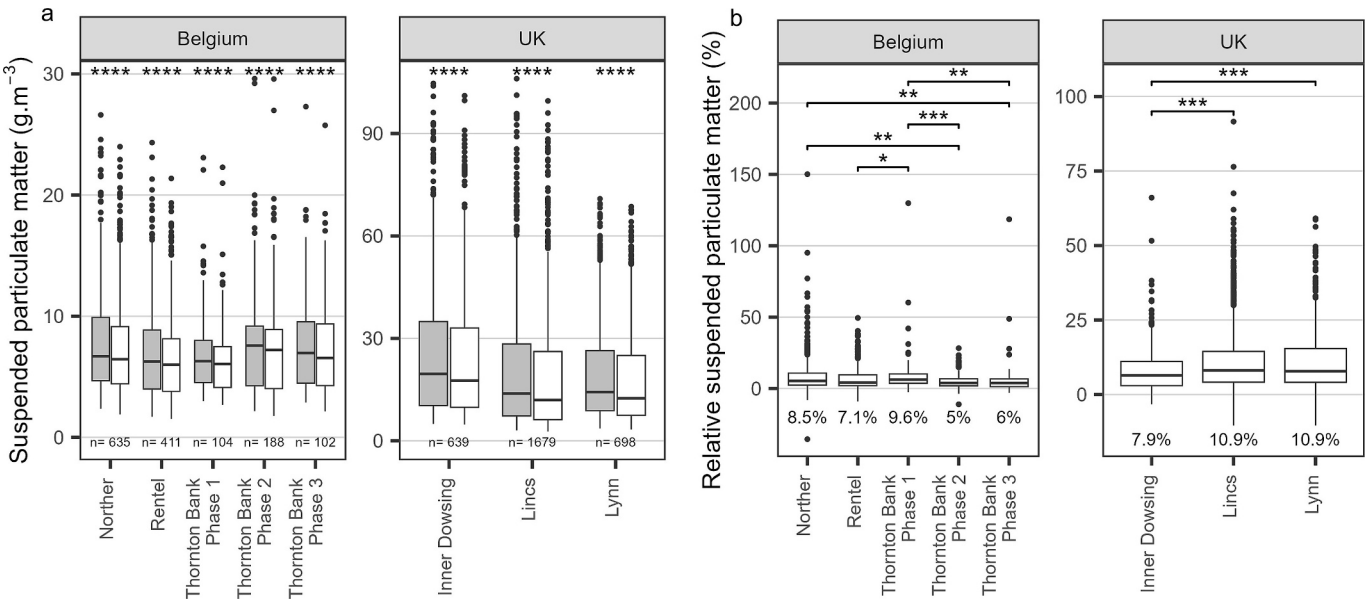

Fig. 5. (a) SPM concentration downstream (grey) and upstream (white) of the turbines per wind farm in Belgium and the UK (n = sample size). Comparisons between upstream and downstream are displayed at the top of each pair of boxes (Wilcoxon signed-rank test). (b) Relative SPM concentration ($\%_{SPM}$) per wind farm in Belgium and the UK (averaged $\%_{SPM}$ displayed below each box). Comparisons are displayed at the top of the plot (Dunn's Test) and mean values are displayed below each box. Significance: * = *p*-value <0.05, ** = p-value <0.01, *** = p-value <0.001, **** = p-value <0.0001.

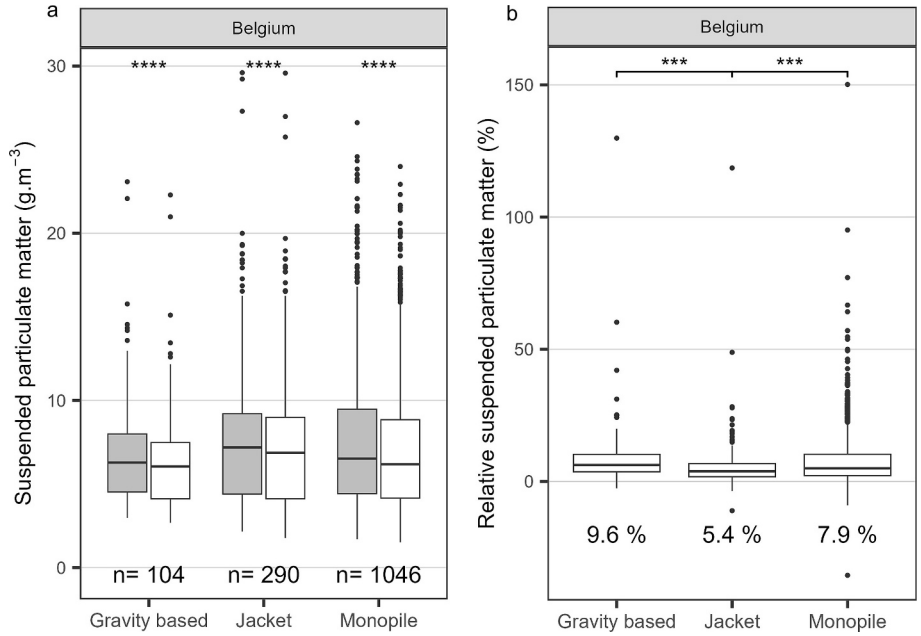

Fig. 6. (a) SPM concentration downstream (grey) and upstream (white) of the turbines per type of foundation in Belgium (n = sample size). Comparisons between upstream and downstream are displayed at the top of each pair of boxes (Wilcoxon signed-rank test). (b) Relative SPM concentration ($\%_{SPM}$) per type of foundation in Belgium (averaged $\%_{SPM}$ displayed below each box). Comparisons are displayed at the top of the plot (Dunn's Test) and mean values are displayed below each box. Significance: *** = p-value <0.001, **** = p-value <0.0001.

with a Δ_{SPM} respectively of 0.16 g m^{-3} (+ 3.6 %), and − 0.04 g m^{-3} (− 0.5 %). On this transect, D0, D7, and D8 are jacket foundations while the others are gravity-based. The wind model provided the same wind speed (9.7 m · s^{-1}) and the current model provided a similar current velocity (0.3 to 0.4 m · s^{-1}), wind wave height (1.1 m) and swell height (0.9 m) applied to every turbine in this scene. Between the turbines, the water depth becomes shallower from turbine D8 to D0, with this last adjacent to a steep slope going from −15 m to −33 m depth in 500 m horizontal diatance. Finally, a gradient of increasing background SPM can be observed from north-west to south-east. This background SPM decreases when reaching the drop in bathymetry, just next to turbine D0 on the transect. It is important to note that this pattern, following the trench, could be noted on several images when the current came from the north-east. This example showed the variability of sediment wakes between turbines as well as the natural variability in a small area.

4. Discussion

A sediment concentration increase due to turbulence enhanced by the underwater structures was observed and quantified in the wake of

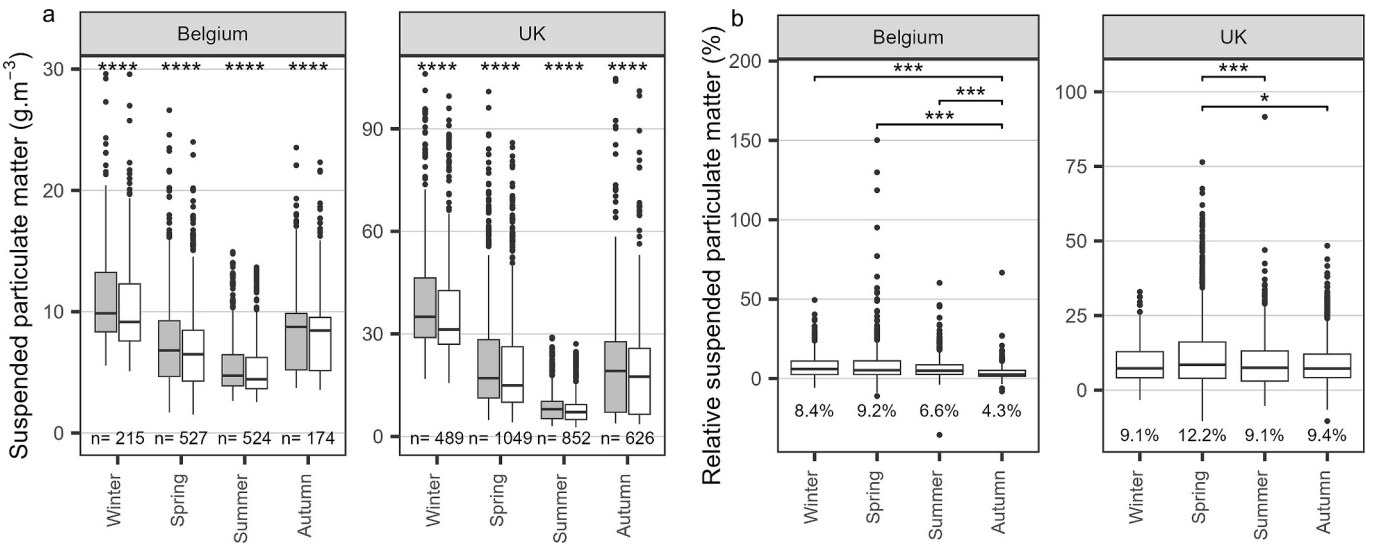

Fig. 7. (a) SPM concentration downstream (grey) and upstream (white) of the turbines per season in Belgium and the UK (n = sample size). Comparisons between upstream and downstream are displayed at the top of each pair of boxes (Wilcoxon signed-rank test). (b) Relative SPM concentration (%$_{SPM}$) per season in Belgium and the UK (averaged %$_{SPM}$ displayed below each box). Comparisons are displayed at the top of the plot (Dunn's Test) and mean values are displayed below each box. Significance: * = p-value <0.05, *** = p-value <0.001, **** = p-value <0.0001.

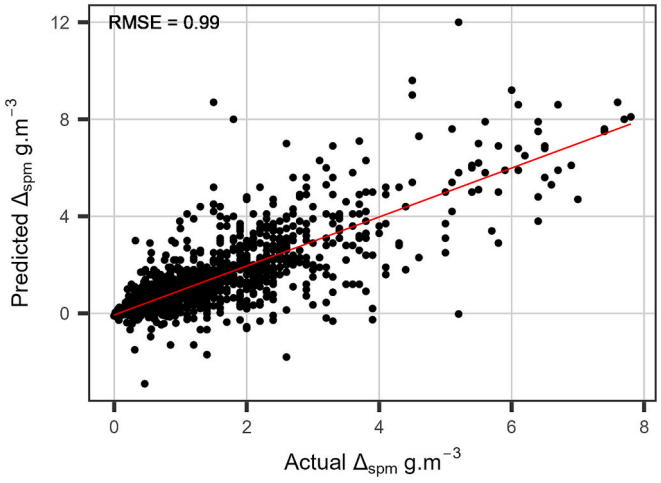

Fig. 8. Validation of the random forest model applied to a third of the dataset (R^2 = 0.65). The red line shows the linear regression. Δ_{SPM} is calculated from Eq. (3).

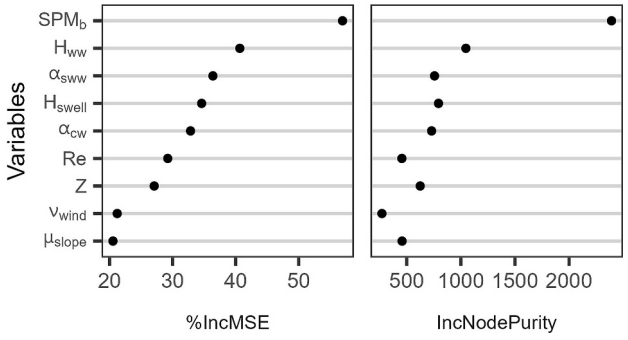

Fig. 9. Variables used in the RF model: background SPM concentration (SPM_b), wind wave height (H_{ww}), difference swell and wind wave direction (α_{sww}), swell height (H_{swell}), the difference between current and wind direction (α_{cw}), Reynolds number (Re), water depth (Z), wind speed (v_{wind}), and the averaged slope 1 km around the turbine (μ_{slope}). On the left: Relative increase in MSE (% IncMSE) if the variable was removed from the model, in other words, measures the importance of the variable. On the right: Increase in node purities (IncNodePurity) of the variables used in the RF model.

OSW turbines using satellite remote sensing methods. The wake's intensity depended on the characteristics of the foundation structure, and physical forces applied to it. A clear seasonal pattern of sediment concentration was also observed upstream of the turbines. With knowledge of the foundation type and diameter, and hydrodynamic and wind regimes, the wake intensity can be predicted with accuracy (RMSE = 0.99).

4.1. Satellite and Copernicus data

Sediment wakes have been observed within the two study sites (Belgium and UK) using the Sentinel-2 and Landsat-8/9 virtual constellation. Both data sources have been used in the past to study SPM concentration and shown to be suitable (Dogliotti et al., 2015; Groom et al., 2019; Luo et al., 2018; Nechad et al., 2010; Tavora et al., 2023; Vanhellemont and Ruddick, 2014, 2015). However, it is important to note that most of the very high wind speed or wave height satellite scenes were found to be unsuitable due to cloud cover or sun-glint (about 28 % of the initially selected images were used in the end), and thus, SPM concentration within sediment wakes during stormy weather with rough seas is still unknown. This limitation is well-known for optical remote sensing and highlights the need for in-situ measurement to fill in the gap in data regarding natural variability (Fettweis et al., 2019). Environmental data layers acquired from CMEMS provided useful insight into the physical parameters that can affect SPM dynamics. The current model provided an accurate current direction, which allowed the automatic selection of the wedge containing the wake to be coded. However, on average, the selected wedges (containing the highest SPM concentration out of 11 wedges initially measured) had an angle of 23° with the current direction predicted by the CMEMS model. The model could have some slight errors, but this difference also could demonstrate the impact of wind and local bathymetry on the wake direction.

4.2. Geographical limitations

The novel geospatial method using wedges developed in this study allowed the identification and quantification of sediment wakes. This

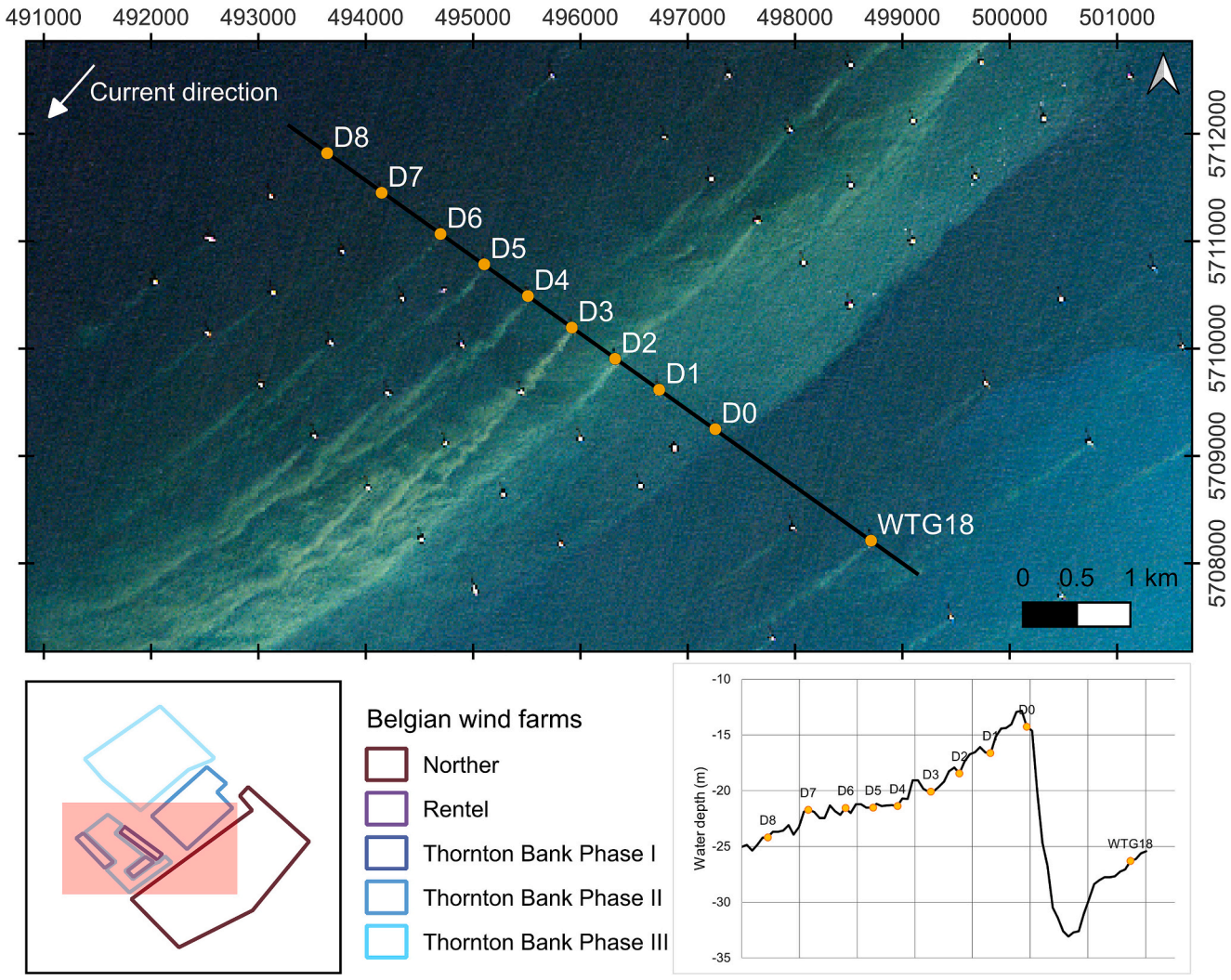

Fig. 10. RGB Sentinel-2A scene (acquisition date: 31/03/2020) showing sediment wakes in the Belgian site. The bathymetric profile at the bottom of the figure is represented by the transect (black line) going from the D8 to the WTG18 turbines.

method focused on the 100 m to 350 m range from the turbines and allowed the comparison between the upstream and downstream SPM concentration. However, several limitations of the method were highlighted. First, the pixels within the selected wedges were averaged, and having a wake evenly filling every pixel of a wedge is uncommon. Therefore, the averaging may have led to an underestimation of the SPM concentration within the wakes as some water pixels from outside the wake were also selected. Consequently, the wake intensities highlighted in this study would likely be higher if measured directly in the field e.g. from a ship located downstream of a foundation. Second, only some of the turbines in the two sites were used, depending on the current direction to avoid the sheltering caused by the wake of another structure. It was visible in many satellite images that several wakes could align together to produce a cascading effect (the wakes of the last row being more intense than the wakes of the first one). In addition, the wave height is reduced each time the flow encounters a new turbine leading to waves received by the last row of turbines being 17 % less than the first one (van der Molen et al., 2014). The same conjecture can be made regarding wind speed. A decrease in wind speed can be observed in the form of wind wakes, reducing the wind received by the turbines sheltered by another one (Bärfuss et al., 2021; Christiansen and Hasager, 2005). Thus, the sheltered turbines could present both more SPM concentration upstream and downstream but also receive weaker hydrodynamic and wind forces which are not present in the models used, which miss local-scale ocean stability in the context of wakes. Consequently, this study does not show the accumulation of sediment wakes throughout a wind farm but the effect of clearly-identifiable single structures only.

4.3. *Shape and size of a turbine*

As found in this study and the literature, sediment wakes can be several kilometres long (Baeye and Fettweis, 2015; Vanhellemont and Ruddick, 2014). This study highlighted that on average, the SPM concentration between 100 m and 350 m downstream of the turbines was 9.4 % higher than upstream of the turbines. Even though Brandao et al. (2023) did not show a regional scale increase in SPM concentration around the wind farms, an inter-farm variability has been demonstrated in this study. A significant difference in SPM concentration could be due to the foundation type with a greater SPM concentration being associated with gravity-based and monopile-based structures. Indeed, the wider the foundation or the faster the current, the higher the *Re*, increasing the erosion at the base and injecting turbulence into the water column (Sumer et al., 2001; Taneda, 1956). This turbulence enhances a Kármán vortex redistributing the sediment toward the surface (Bailey et al., 2024). However, the entire jacket foundation was not considered for the Reynolds number (*Re*) calculation – only the diameter of one out of the four pin legs was considered as the interaction between the four

legs is hard to predict. The jacket foundations used for Thornton Bank Phase II and III present a high pile-diameter-to-gap ratio (G/D) with 2 m pin piles spaced 18 m apart (Bolle et al., 2012). This high G/D allows the flow to run in between the pin piles, reducing the downward flow reaching the seabed and thus, reducing the scour depth (Sumer et al., 2001). The gravity-based structures present a slope angle of 63° with the seabed while monopiles are vertical structures presenting an angle of 90° (Peire et al., 2009). It was shown that if the flow reaches a structure with a slope, the erosion of the seabed is reduced compared to the flow reaching a structure perpendicularly (Sumer et al., 2001). This means that even if gravity-based foundations are massive, their sloping surface might reduce the turbulence leading to no significant difference in $\%_{SPM}$ with the monopiles despite their several times wider diameter. Also, gravity-based foundations in the Belgian sites are all protected by rock armour at the base limiting local seabed erosion (Peire et al., 2009) by reducing flow turbulence at the base of the foundation (Bradbury et al., 2024).

4.4. Prediction of wake appearance

The use of a RF model allowed the prediction of resuspended sediment by the studied bottom-fixed turbines. Using an RF model to predict sediment concentration has been proven to be effective in other studies (Al-Mukhtar, 2019; Walsh et al., 2017). Yet, the relationship between SPM concentration and environment and physical variables within OSW farms was shown to be complex (Brandao et al., 2023). The variables used to build the model were found to be important in the decision trees, regarding the RF nodes' purity. The seabed type could be important but was not considered in the RF model due to a lack of fine-scale data at the resolution of the seabed surrounding individual structures. EMODNet has gathered and formatted seabed data from different countries following Folk's classification, but these data were not precise enough. This study would have required accurate information on the type of sediment and grain size at the base of each turbine, therefore, at a very small scale. However, the type of sediment is expected to impact the wakes as different grain sizes and cohesiveness of the sediment will lead to different resuspension regimes (Baeye et al., 2011). Another factor not considered was biofouling, due to the so-called "reef effect" whereby benthic organisms colonise the surfaces of the foundation, often reaching very high densities. Colonisation on the foundation increases its roughness, especially with blue mussels which can sometimes accumulate at up to 1.4 tons of dry biomass per structure (Ameryoun et al., 2019; Maar et al., 2009). This mussel aggregation was estimated to add 50 cm to jacket pin legs constructed 4 years before, hence increasing the diameter of the foundation (Hutchison et al., 2020). It is hard to predict how this biofouling affects the flow turbulence; the increased roughness and diameter are likely to enhance turbulence, however, its randomness due to species shape and size or the multi-layering of several species makes the impact of biofouling on flow disturbance still a question of debate (Maduka et al., 2023). The presence of a mussel ring could also enhance the number of particles (pellets or pseudofeces) downstream of the piles (Reichart et al., 2017), even though this was not observed by Bailey et al., 2024. Unfortunately, no presently-available dataset provides information on the thickness or the roughness of the mussel layer on the studied wind turbines. As biofouling develops over time on the structure (Degraer et al., 2020), the age of the turbines when the satellite scene was taken was however considered. Years since construction did not play a major role in the RF model and, therefore, was not kept in the final model.

4.4.1. Hydrodynamic and wind forcings

Hydrodynamic and wind forcings had a strong influence on the final RF model with variables of high importance such as wave height, current, and wind direction. High current velocity is known for increasing turbulence around the turbine's foundation, leading to sediment resuspension and scouring. Waves are also known to induce shear stress leading to a peak in SPM concentration during or just after a high wave episode (Dobrynin et al., 2010; Puls et al., 1999). Likewise, wind speed is expected to play a role in sediment resuspension as the wind was shown to enhance wind-induced flows (Baeye et al., 2011; Eleveld et al., 2008; Jago and Jones, 1998; Jones et al., 1998). Additionally, those forcings can act in synergy. It was shown that wind waves and swell together impacted the formation of scour at the base of the foundations and therefore, demonstrated more turbulence (Sumer et al., 2001). Further, Baeye et al. (2011) revealed that natural variability/background SPM concentration is mainly driven by tidal forces but significantly impacted by wind-induced flow. When both forces ran in the same direction, the SPM concentration observed was higher, and current and wind waves can move sediment from distant areas toward some clear water locations, increasing the SPM_b. This was described by the variables α_{sww} and α_{cw} in the RF model showing a strong interaction between hydrodynamic and wind forcings on the water column and likely to modify the wake's intensity and direction. Also, using these angles as variables in the model allowed the study of both sites together regardless of the general current regime (as the current direction is highly site-specific depending on the current and tidal regime of this location).

4.4.2. Bathymetry and seabed morphology

Aside from physical forces, the water depth (Z) and seabed morphology (μ_{slope}) were shown to be of importance in the RF model. A shallow bathymetry is likely to increase turbidity in the area, but also the current velocity, as the same volume of water passes through a smaller space. In some cases, no sediment wakes were observed downstream of the turbines located on a slope or near a changing bathymetry. Seabed morphology could induce changes in the flow system making the whole area more turbulent and turbid. In that case, the effect of the structures and water flow could be negligible compared to natural variability. Bathymetry is one of the criteria for choosing the type of foundation needed: jacket foundations are more likely to be installed further offshore than monopiles and gravity-based foundations (Bailey et al., 2014). In deeper areas, the previous forcings presented such as wind waves, swell, and wind speed are less important as the wave orbital velocity cannot reach the seabed while in shallow areas, waves are a major component of vertical mixing (Dobrynin et al., 2010). The seabed morphology, μ_{slope}, also showed some impact on wake intensity in the model. Mercier and Guillou (2021) showed that seabed morphology, especially, large underwater sandbanks can modify the current regime. This could potentially explain why some turbines, located nearby complex seabed morphology, showed reduced or absent wakes.

4.5. Underwater light changes

Sediment wakes can be noticed all year round but with different intensities that follow a clear seasonal pattern. This seasonal pattern is well-known as background SPM changes naturally, driven by physical and biological forces, affecting underwater light. Turbid wakes generated by OSW turbines can also modify the underwater light field to a smaller extent. A general reduction of the euphotic zone (Z_{eu}) of 5.7 % was observed in the studied wakes (3 % and 5.5 % respectively for the Belgian and the UK sites). It is important to highlight again that this study only covers turbines not in the wake of another turbine. The reduction of Z_{eu} could therefore be more important for the wakes resulting in a cascading effect. However, the effects of these small changes remain to be seen, especially regarding the natural variability already occurring in coastal seas (Bailey et al., 2024).

5. Conclusion

Satellite remote sensing techniques were used to build an understanding of the impact of OSW structures on sediment resuspension. This study offered a qualitative and quantitative assessment of SPM concentration downstream of OSW turbines. Sediment wakes were shown to

differ in intensity between wind farms, and to show seasonality. More intense wakes were observed downstream of gravity-based and monopile foundations than jacket foundations due to their shape and size. Wake intensity can be predicted for bottom fixed turbines depending on the background turbidity, their size, the hydrodynamic and wind forcings applied to the structure, and the seabed morphology. Predictions could help in carrying out the environmental impact assessment at the early stage of a wind farm design and assess feasibility for potential multi-use projects with other stakeholders such as aquaculture. Further work could look at how sediment wakes can add up when turbines are aligned with the current direction, as well as better quantify the effect of turbid wakes on underwater irradiance and primary production. This would help to understand the potential cumulative effect of sediment wakes within wind farms, especially as the number of wind farms at sea will keep growing, moving more into stratified waters, to reach the Net Zero target by 2050.

CRediT authorship contribution statement

Enora M. Lecordier: Writing – original draft, Methodology, Investigation, Formal analysis, Conceptualization. **Pierre Gernez:** Writing – review & editing, Validation, Supervision, Methodology, Formal analysis. **Krysia Mazik:** Writing – review & editing, Validation, Supervision, Formal analysis. **Katharine York:** Writing – review & editing, Supervision, Formal analysis, Data curation, Conceptualization. **Rodney M. Forster:** Writing – review & editing, Supervision, Methodology, Formal analysis, Conceptualization.

Declaration of competing interest

The authors declare that they have no known competing financial interests or personal relationships that could have appeared to influence the work reported in this paper.

Acknowledgements

This work was conducted under the Aura CDT program, funded by the Engineering and Physical Sciences Research Council (EPSRC), and Natural Environment Research Council (NERC), grant number EP/S023763/1 and project reference 2610351, and the project eSWEETS: Enabling Sustainable Wind Energy Expansion in Seasonable Seas, NERC, grant number NE/X004953/1. This research was sponsored by Offshore Renewable Energy Catapult. The work was made possible due to financial assistance and technical expertise offered by the organisation. We would like to acknowledge Viper High Performing Computer of the University of Hull for their help in processing the satellite images. Also, we are grateful to Dr. Quinten Vanhellemont for his expertise and help in using the ACOLITE software.

Appendix A. Supplementary data

Supplementary data to this article can be found online at https://doi.org/10.1016/j.scitotenv.2025.178814.

Data availability

Data will be made available on request.

References

Al-Mukhtar, M., 2019. Random forest, support vector machine, and neural networks to modelling suspended sediment in Tigris River-Baghdad. Environ. Monit. Assess. 191 (11), 673. https://doi.org/10.1007/s10661-019-7821-5.

Ameryoun, H., Schoefs, F., Barillé, L., Thomas, Y., 2019. Stochastic modeling of forces on jacket-type offshore structures colonized by marine growth. Journal of Marine Science and Engineering 7 (5). https://doi.org/10.3390/jmse7050158.

Amini, A., Melville, B.W., Ali, T.M., Ghazali, A.H., 2012. Clear-water local scour around pile groups in shallow-water flow. J. Hydraul. Eng. 138 (2), 177–185. https://doi.org/10.1061/(asce)hy.1943-7900.0000488.

Austin, M., Unsworth, C., Van Landeghem, K., & Lincoln, B. (in-press). Enhanced bed shear stress and mixing in the tidal wake of an offshore wind turbine monopile. Ocean Sci., 17. doi:https://doi.org/10.5194/egusphere-2024-205.

Baeye, M., Fettweis, M., 2015. In situ observations of suspended particulate matter plumes at an offshore wind farm, southern North Sea. Geo-Mar. Lett. 35 (4), 247–255. https://doi.org/10.1007/s00367-015-0404-8.

Baeye, M., Fettweis, M., Voulgaris, G., Van Lancker, V., 2011. Sediment mobility in response to tidal and wind-driven flows along the Belgian inner shelf, southern North Sea. Ocean Dyn. 61 (5), 611–622. https://doi.org/10.1007/s10236-010-0370-7.

Bailey, H., Brookes, K.L., Thompson, P.M., 2014. Assessing environmental impacts of offshore wind farms: lessons learned and recommendations for the future. Aquatic Biosystems 10 (1), 8. https://doi.org/10.1186/2046-9063-10-8.

Bailey, L.P., Dorrell, R.M., Kostakis, I., McKee, D., Parsons, D., Rees, J., Strong, J., Simmons, S., Forster, R., 2024. Monopile-induced turbulence and sediment redistribution form visible wakes in offshore wind farms. Front. Earth Sci. 12. https://doi.org/10.3389/feart.2024.1383726.

Bärfuss, K., Schulz-Stellenfleth, J., Lampert, A., 2021. The impact of offshore wind farms on sea state demonstrated by airborne LiDAR measurements. Journal of Marine Science and Engineering 9 (6). https://doi.org/10.3390/jmse9060644.

Belgiu, M., Drăguţ, L., 2016. Random forest in remote sensing: a review of applications and future directions. ISPRS J. Photogramm. Remote Sens. 114, 24–31. https://doi.org/10.1016/j.isprsjprs.2016.01.011.

Bolle, A., De Winter, J., Goossens, W., Haerens, P., Dewaele, G., 2012. Scour monitoring around offshore jackets and gravity based foundations. In: Proceedings of the sixth international conference on scour and erosion, icse, 6.

Bolle, A., Mathys, M., Haerens, P., 2013. How the Belgian wind farm business made us discover the challenging environment of marine sand dunes. In: Proceedings of 4th international con ference on marine and river dune dynamics, marid iv, pp. 45–52.

Bradbury, M., McLelland, S., Dorell, R., Marten, K., Whitehouse, R., 2024. Understanding the effectiveness of scour mitigation techniques at offshore windfarms using experimental modelling. In: EGU general assembly 2024. EGU24–17966. https://doi.org/10.5194/egusphereegu24-17966.

Brandao, I.L.S., van der Molen, J., van der Wal, D., 2023. Effects of offshore wind farms on suspended particulate matter derived from satellite remote sensing. Sci. Total Environ. 866, 161114. https://doi.org/10.1016/j.scitotenv.2022.161114.

Breiman, L., 2001. Random forests. Mach. Learn. 45, 5–32. https://doi.org/10.1023/A:1010933404324.

Cazenave, P.W., Torres, R., Allen, J.I., 2016. Unstructured grid modelling of offshore wind farm impacts on seasonally stratified shelf seas. Prog. Oceanogr. 145, 25–41. https://doi.org/10.1016/j.pocean.2016.04.004.

Chen, J., Kim, M.-H., 2021. Review of recent offshore wind turbine research and optimization methodologies in their design. Journal of Marine Science and Engineering 10 (1). https://doi.org/10.3390/jmse10010028.

Chirosca, A.-M., Rusu, L., Bleoju, A., 2022. Study on wind farms in the North Sea area. Energy Rep. 8, 162–168. https://doi.org/10.1016/j.egyr.2022.10.244.

Christiansen, M.B., Hasager, C.B., 2005. Wake effects of large offshore wind farms identified from satellite SAR. Remote Sens. Environ. 98 (2–3), 251–268. https://doi.org/10.1016/j.rse.2005.07.009.

C-Power, 2024. Technology foundations. Retrieved June 27, 2024, from. https://c-power.be/en/. technology/Foundations.

Degraer, S., Carey, D., Coolen, J., Hutchison, Z., Kerckhof, F., Rumes, B., Vanaverbeke, J., 2020. Offshore wind farm artificial reefs affect ecosystem structure and functioning: a synthesis. Oceanography 33 (4), 48–57. https://doi.org/10.5670/oceanog.2020.405.

Dinno, A., 2015. Nonparametric pairwise multiple comparisons in independent groups using Dunn's test. Stata J. 15 (1), 292–300. https://doi.org/10.1177/1536867X1501500117.

Dobrynin, M., Gayer, G., Pleskachevsky, A., Günther, H., 2010. Effect of waves and currents on the dynamics and seasonal variations of suspended particulate matter in the North Sea. J. Mar. Syst. 82 (1–2), 1–20. https://doi.org/10.1016/j.jmarsys.2010.02.012.

Dogliotti, A.I., Ruddick, K.G., Nechad, B., Doxaran, D., Knaeps, E., 2015. A single algorithm to retrieve turbidity from remotely-sensed data in all coastal and estuarine waters. Remote Sens. Environ. 156, 157–168. https://doi.org/10.1016/j.rse.2014.09.020.

Dunn, O., 1961. Multiple comparisons among means. J. Am. Stat. Assoc. 56 (293), 52–64. https://doi.org/10.1080/01621459.1961.10482090.

EGS International Ltd, 2016. Lincs Offshore Wind Farm - Post Construction Geophysical Survey 2016. EGS International Ltd. The Crown Estate. https://www.marinedataexchange.co.uk/details/TCE-947/2016-egs-lincs-geophysical-survey.

EGS International Ltd, 2017, June. Lincs Offshore Wind Farm - LS23 & LS65 Clearance Survey 2017. EGS International Ltd. The Crown Estate. https://www.marinedataexchange.co.uk/details/TCE-959/2017-egs-lincs-ls23-and-ls65-clearance-survey.

EGS International Ltd, 2017, August. Lincs Offshore Wind Farm - Post Construction Geophysical Survey 2017b. EGS International Ltd. The Crown Estate. https://www.marinedataexchange.co.uk/details/TCE-910/2017-egs-lincs-geophysical-survey.

Eleveld, M.A., Pasterkamp, R., van der Woerd, H.J., Pietrzak, J.D., 2008. Remotely sensed seasonality in the spatial distribution of sea-surface suspended particulate matter in the southern North Sea. Estuar. Coast. Shelf Sci. 80 (1), 103–113. https://doi.org/10.1016/j.ecss.2008.07.015.

Fettweis, M., Riethmüller, R., Verney, R., Becker, M., Backers, J., Baeye, M., Chapalain, M., Claeys, S., Claus, J., Cox, T., Deloffre, J., Depreiter, D., Druine, F., Flöser, G., Grünler, S., Jourdin, F., Lafite, R., Nauw, J., Nechad, B., Röttgers, R.,

Sottolichio, A., Van Engeland, T., Vanhaverbeke, W., Vereecken, H., 2019. Uncertainties associated with in situ high-frequency long-term observations of suspended particulate matter concentration using optical and acoustic sensors. Prog. Oceanogr. 178. https://doi.org/10.1016/j.pocean.2019.102162.

Fitch-Roy, O., 2015. An offshore wind union? Diversity and convergence in European offshore wind governance. Clim. Pol. 16 (5), 586–605. https://doi.org/10.1080/14693062.2015.1117958.

Floeter, J., van Beusekom, J.E.E., Auch, D., Callies, U., Carpenter, J., Dudeck, T., Eberle, S., Eckhardt, A., Gloe, D., Hänselmann, K., Hufnagl, M., Janßen, S., Lenhart, H., Möller, K.O., North, R.P., Pohlmann, T., Riethmüller, R., Schulz, S., Spreizenbarth, S., Temming, A., Walter, B., Zielinski, O., Möllmann, C., 2017. Pelagic effects of offshore wind farm foundations in the stratified North Sea. Prog. Oceanogr. 156, 154–173. https://doi.org/10.1016/j.pocean.2017.07.003.

Forster, R., 2018. The effect of monopile-induced turbulence on local suspended sediment pattern around the UK wind farms. An IECS report to The Crown Estate 1–8. https://cms.ore.catapult.org.uk/wp-content/uploads/2018/12/The-Effect-of-Monopile-InducedTurbulence-on-Local-Suspended-Sediment-Pattern-around-UK-Wind-Farms.pdf.

Gislason, P.O., Benediktsson, J.A., Sveinsson, J.R., 2006. Random forests for land cover classification. Pattern Recogn. Lett. 27 (4), 294–300. https://doi.org/10.1016/j.patrec.2005.08.011.

Global Wind Atlas 3.0, 2023. Global wind atlas. Retrieved June 27, 2024, from. https://globalwindatlas.info.

Groom, S., Sathyendranath, S., Ban, Y., Bernard, S., Brewin, R., Brotas, V., Brockmann, C., Chauhan, P., Choi, J.-K., Chuprin, A., Ciavatta, S., Cipollini, P., Donlon, C., Franz, B., He, X., Hirata, T., Jackson, T., Kampel, M., Krasemann, H., Wang, M., 2019. Satellite Ocean colour: current status and future perspective. Front. Mar. Sci. 6. https://doi.org/10.3389/fmars.2019.00485.

Hademenos, V., Stafleu, J., Missiaen, T., Kint, L., Van Lancker, V.R.M., 2019. 3D subsurface characterisation of the Belgian continental shelf: a new voxel modelling approach. Neth. J. Geosci. 98. https://doi.org/10.1017/njg.2018.18.

Hoeser, T., Feuerstein, S., Kuenzer, C., 2022. DeepOWT: a global offshore wind turbine data set derived with deep learning from Sentinel-1 data. Earth System Science Data 14 (9), 4251–4270. https://doi.org/10.5194/essd-14-4251-2022.

Hutchison, Z.L., LaFrance Bartley, M., Degraer, S., English, P., Khan, A., Livermore, J., Rumes, B., W., K. J., 2020. Offshore wind energy and habitat changes. Oceanography 33 (4), 58–69.

IPCC, 2011. Summary for policymakers. In: Edenhofer, O., Pichs-Madruga, R., Sokona, Y., Seyboth, K., Matschoss, P., Kadner, S., Zwickel, T., Eickemeier, P., Hansen, G., Schlömer, S., von Stechow, C. (Eds.), IPCC Special Report on Renewable Energy Sources and Climate Change Mitigation. Cambridge University Press.

Jago, C.F., Jones, S.E., 1998. Observation and modelling of the dynamics of benthic fluff resuspended from a sandy bed in the southern North Sea. Cont. Shelf Res. 18, 1255–1282. https://doi.org/10.1016/S0278-4343(98)00043-0.

Jones, S.E., Jago, C.F., Bale, A.J., Chapman, D., Howland, R.J.M., Jackson, J., 1998. Aggregation and resuspension of suspended particulate matter at a seasonally stratified site in the southern North Sea: physical and biological controls. Cont. Shelf Res. 18, 1283–1309. https://doi.org/10.1016/S0278-4343(98)00044-2.

Kint, L., Hademenos, V., De Mol, R., Stafleu, J., van Heteren, S., Van Lancker, V., 2020. Uncertainty assessment applied to marine subsurface datasets. Q. J. Eng. Geol. Hydrogeol. 54 (1). https://doi.org/10.1144/qjegh2020-028.

Kuhn, C., de Matos Valerio, A., Ward, N., Loken, L., Sawakuchi, H.O., Kampel, M., Richey, J., Stadler, P., Crawford, J., Striegl, R., Vermote, E., Pahlevan, N., Butman, D., 2019. Performance of Landsat-8 and Sentinel-2 surface reflectance products for river remote sensing retrievals of chlorophyll-a and turbidity. Remote Sens. Environ. 224, 104–118. https://doi.org/10.1016/j.rse.2019.01.023.

Lawrence, R.L., Wood, S.D., Sheley, R.L., 2006. Mapping invasive plants using hyperspectral imagery and Breiman Cutler classifications (randomforest). Remote Sens. Environ. 100 (3), 356–362. https://doi.org/10.1016/j.rse.2005.10.014.

Lee, Z., Carder, K.L., Arnone, R.A., 2002. Deriving inherent optical properties from water color: a multiband quasi-analytical algorithm for optically deep waters [Lee, ZhongPing Carder, Kendall L Arnone, Robert A eng 2002/09/25 Applied Optics. 2002 Sep 20;41(27):5755-72. doi: 10.1364/ao.41.005755.]. Appl. Optics 41 (27), 5755–5772. https://doi.org/10.1364/ao.41.005755.

Luo, Y., Doxaran, D., Ruddick, K., Shen, F., Gentili, B., Yan, L., Huang, H., 2018. Saturation of water reflectance in extremely turbid media based on field measurements, satellite data and bio-optical modelling. Opt. Express 26 (8), 10435–10451. https://doi.org/10.1364/OE. 26.010435.

Maar, M., Bolding, K., Petersen, J.K., Hansen, J.L.S., Timmermann, K., 2009. Local effects of blue mussels around turbine foundations in an ecosystem model of Nysted offshore wind farm, Denmark. Journal of Sea Research 62 (2–3), 159–174. https://doi.org/10.1016/j. seares.2009.01.008.

Maciel, F.P., Pedocchi, F., 2021. Evaluation of ACOLITE atmospheric correction methods for Landsat-8 and Sentinel-2 in the Río de la Plata turbid coastal waters. Int. J. Remote Sens. 43 (1), 215–240. https://doi.org/10.1080/01431161.2021.2009149.

Maduka, M., Schoefs, F., Thiagarajan, K., Bates, A., 2023. Hydrodynamic effects of biofouling-induced surface roughness – review and research gaps for shallow water offshore wind energy structures. Ocean Eng. 272. https://doi.org/10.1016/j.oceaneng.2023.113798.

Matutano, C., Negro, V., López-Gutiérrez, J.-S., Esteban, M.D., 2013. Scour prediction and scour protections in offshore wind farms. Renew. Energy 57, 358–365. https://doi.org/10.1016/j.renene.2013.01.048.

Mercier, P., Guillou, S., 2021. The impact of the seabed morphology on turbulence generation in a strong tidal stream. Phys. Fluids 33 (5). https://doi.org/10.1063/5.0047791.

Miles, J., Martin, T., Goddard, L., 2017. Current and wave effects around windfarm monopile foundations. Coastal Engineering 121, 167–178. https://doi.org/10.1016/j.coastaleng.2017.01.003.

van der Molen, J., Smith, H.C.M., Lepper, P., Limpenny, S., Rees, J., 2014. Predicting the largescale consequences of offshore wind turbine array development on a North Sea ecosystem. Cont. Shelf Res. 85, 60–72. https://doi.org/10.1016/j.csr.2014.05.018.

Nechad, B., Ruddick, K.G., Park, Y., 2010. Calibration and validation of a generic multisensor algorithm for mapping of total suspended matter in turbid waters. Remote Sens. Environ. 114 (4), 854–866. https://doi.org/10.1016/j.rse.2009.11.022.

Negro, V., López-Gutiérrez, J.-S., Esteban, M.D., Alberdi, P., Imaz, M., Serraclara, J.-M., 2017. Monopiles in offshore wind: preliminary estimate of main dimensions. Ocean Eng. 133, 253–261. https://doi.org/10.1016/j.oceaneng.2017.02.011.

Norro, A., 2018. Mitigation measure for offshore wind farm piling sound: a single big bubble curtain as mitigation measure for offshore wind farm piling sound in Belgian waters. In: Memoires on the marine environment, pp. 19–25.

Peire, K., Nonneman, H., Bosschem, E., 2009. Gravity base foundations for the Thornton Bank offshore wind farm. Terra and Aqua 115 (115), 19–29.

Pipeshield, 2024. Concrete mattress. Retrieved November 26, 2024, from. https://pipeshield.com/products/concrete-mattresses.

Puls, W., Beusekom, J., Brockmann, U., Doerffer, R., Hentschke, U., König, P., Murphy, D., Mayer, B., Müller, A., Pohlmann, T., Reimer, A., Schmidt-Nia, R., Sündermann, J., 1999. SPM concentrations in the German Bight: comparison between a model simulation and measurements. Deutsche Hydrographische Zeitschrift 51 (2/3), 221–244. https://doi.org/10.1007/bf02764175.

QGIS.org, 2024. Qgis geographic information system. Retrieved June 27, 2024, from. http://www.qgis.org.

R Core Team, 2024. R: A Language and Environment for Statistical Computing. R Foundation for Statistical Computing, Vienna, Austria. https://www.R-project.org/.

Ranghetti, L., Boschetti, M., Nutini, F., Busetto, L., 2020. "sen2r": an R toolbox for automatically downloading and preprocessing Sentinel-2 satellite data. Comput. Geosci. 139. https://doi.org/10.1016/j.cageo.2020.104473.

Reichart, G., Mienis, F., Duineveld, G., Stoetaert, K., Fillipidi, A., 2017. Measuring the SHADOW of an artificial structure in the North Sea and its effect on the surrounding soft bottom community. NIOZ Royal Netherlands Institute for Sea Research and Utrecht University. https://insitenorthsea.org/projects/measuring-the-shadow-of-artificial-structures-in-thenorth-sea-and-its-effect-on-the-surrounding-soft-bottom-community.

Rogan, C., Miles, J., Simmonds, D., Iglesias, G., 2016. The turbulent wake of a monopile foundation. Renew. Energy 93, 180–187. https://doi.org/10.1016/j.renene.2016.02.050.

RPS, 2014. LID Year 3 Post-Construction Monitoring Summary Report. The Crown Estate.

Schendel, A., Hildebrandt, A., Goseberg, N., Schlurmann, T., 2018. Processes and evolution of scour around a monopile induced by tidal currents. Coastal Engineering 139, 65–84. https://doi.org/10.1016/j.coastaleng.2018.05.004.

Sif, 2024. Products services - references. Retrieved December 12, 2024, from. https://sif-group.com/en/references/.

Sumer, B., Whitehouse, R., Tørum, A., 2001. Scour around coastal structures: a summary of recent research. Coast. Eng. 44 (2), 153–190. https://doi.org/10.1016/S03783839(01)00024-2.

Taneda, S., 1956. Experimental investigation of the wake behind a sphere at low Reynolds numbers. J. Physical Soc. Japan 11 (10), 1104–1108.

Tavora, J., Jiang, B., Kiffney, T., Bourdin, G., Clifton Gray, P., Sander de Carvalho, L., Hesketh, G., Schild, K.M., Faria de Souza, L., Brady, D.C., Boss, E., 2023. Recipes for the derivation of water quality parameters using the high spatial resolution data from sensors on board Sentinel-2a, −2b and Landsat-5, −7, −8, −9 satellites. Journal of Remote Sensing. https://doi.org/10.34133/remotesensing.0049.

The Engineering ToolBox, 2004. Water - dynamic (absolute) and kinematic viscosity vs. temperature and pressure. Retrieved June 27, 2024, from. https://www.engineeringtoolbox.com/water-dynamic-kinematic-viscosity-d_596.html.

Van den Eynde, D., Brabant, R., Fettweis, M., Francken, F., Melotte, J., Sas, M., Van Lancker, V., 2010. Monitoring of hydrodynamic and morphological changes at the C-power and the Belwind offshore wind farm sites: A synthesis. In: Offshore Wind Farms in the Belgian Part of the North Sea. Early Environmental Impact Assessment and Spatio-Temporal Variability. Royal Belgian Institute of Natural Sciences, Management Unit of the North Sea Mathematical Models, pp. 19–36.

Vanhellemont, Q., 2019. Adaptation of the dark spectrum fitting atmospheric correction for aquatic applications of the Landsat and Sentinel-2 archives. Remote Sens. Environ. 225, 175–192. https://doi.org/10.1016/j.rse.2019.03.010.

Vanhellemont, Q., Ruddick, K., 2014. Turbid wakes associated with offshore wind turbines observed with Landsat 8. Remote Sens. Environ. 145, 105–115. https://doi.org/10.1016/j.rse.2014.01.009.

Vanhellemont, Q., Ruddick, K., 2015. Advantages of high quality SWIR bands for ocean colour processing: examples from Landsat-8. Remote Sens. Environ. 161, 89–106. https://doi.org/10.1016/j.rse.2015.02.007.

Walsh, E.S., Kreakie, B.J., Cantwell, M.G., Nacci, D., 2017. A random forest approach to predict the spatial distribution of sediment pollution in an estuarine system. PloS One 12 (7), e0179473. https://doi.org/10.1371/journal.pone.0179473.

Wang, H., Wang, J., Cui, Y., Yan, S., 2021. Consistency of suspended particulate matter concentration in turbid water retrieved from Sentinel-2 MSI and Landsat-8 OLI sensors. Sensors 21 (5). https://doi.org/10.3390/s21051662.

Welzel, M., Schendel, A., Hildebrandt, A., Schlurmann, T., 2019. Scour development around a jacket structure in combined waves and current conditions compared to monopile foundations. Coastal Engineering 152. https://doi.org/10.1016/j.coastaleng.2019.103515.

Welzel, M., Schendel, A., Satari, R., Neuweiler, I., Schlurmann, T., 2024. Spatio-temporal analysis of scour around complex offshore foundations under clear water and live bed conditions. Ocean Eng. 298. https://doi.org/10.1016/j.oceaneng.2024.117042.

WindEurope, 2020. Offshore wind in Europe - key trends and statistics 2019.

Zhang, T., Tian, B., Sengupta, D., Zhang, L., Si, Y., 2021. Global offshore wind turbine dataset. Scientific Data 8 (1), 191. https://doi.org/10.1038/s41597-021-00982-z.